IEEE Access
Multidisciplinary | Rapid Review | Open Access Journal

Received November 1, 2018, accepted November 27, 2018, date of publication December 7, 2018,
date of current version December 31, 2018.

Digital Object Identifier 10.1109/ACCESS.2018.2885356

Planar Phase Gradient Metasurface Antenna With Low RCS

BO LI[1], XIAOBO LIU[2], HONGYU SHI[2], (Member, IEEE), CHUN YANG[1], QI CHEN[1], AND ANXUE ZHANG[2]

[1]Institute of Electronic Engineering, China Academy of Engineering Physics, Mianyang 621999, China
[2]School of Electronics and Information Engineering, Xi'an Jiaotong University, Xi'an 710049, China

Corresponding author: Hongyu Shi (hongyushi@xjtu.edu.cn)

This work was supported in part by the National Natural Science Foundation of China under Grant 61501365 and Grant 61302047, and in part by the China Postdoctoral Science Foundation under Grant 2015M580849.

ABSTRACT A low radar cross section (RCS) planar antenna using phase gradient metasurface is proposed in this paper. The proposed antenna works in the *X*-band and is fed by a parallel plate waveguide power divider. The designed phase gradient metasurface is coplanar with the feeding structure and couples guided waves in the parallel plate waveguide power divider to radiation waves. According to the generalized reflection law, the proposed metasurface is a frequency scanning antenna and the beam direction can be steered slightly from 16.6° to 13°. The proposed antenna is linearly polarized, and however, the RCS is reduced significantly for arbitrary polarized incident waves. The antenna was simulated, fabricated, and measured. The measurement results confirm well with the simulation results.

INDEX TERMS Phase gradient metasurface, low profile, frequency scanning, RCS reduction.

I. INTRODUCTION

Metasurfaces are 2D planar metamaterials consisting of sub-wavelength artificial structures, which could realize some unusual characteristics including asymmetric transmission, beam steering, absorbing, abnormal reflections and so on. Metasurfaces have been applied in stealth devices [1]–[4], cloaking [5], [6], reduction of mutual coupling in antenna arrays [7], [8], polarization steering [9], planar antennas [10], beam controlling [11]–[14], spoof surface plasmon polaritons (SPPs) coupling [15]–[18], etc.

Phase gradient metasurfaces (PGMs) can provide an additional pre-defined wave vector along the phase gradient direction. Such additional pre-defined wave vector is achieved by the non-uniform reflection/transmission phase of each unit cell which is composed of several sub-elements with a gradient phase response to the incident wave. Due to the additional pre-defined wave vector, wave fronts of the reflective/refractive waves can be controlled by the designed phase gradient, for example the anomalous reflections/refractions [19]–[22]. Recently, theoretical and application researchs based on such characteristic of PGMs have been reported. A theoretical polarization insensitive analysis is given in [23]. A planar lens based on a multi-layered PGM was designed for antenna design [24], [25]. This lens transforms a quasi-spherical wave to a plane wave, and the aperture efficiency is greatly improved. In [26], an ultra-thin polarization beam splitter was realized by a tri-layered PGM, which can manipulate two orthonormal linearly polarized waves independently. In addition, spatial propagation waves can be converted to surface waves or spoof SPPs with high efficiency when the additional wave vector supported by PGM is bigger than the one of the incidence. Thus, PGMs can play a role of bridge link between propagating waves and surface waves [27]. This property has been applied for frequency scanning planar metasurface antennas [10], where the feed horn is not coplanared with the PGM which may cause some difficulty for manufacture and integration.

In certain occasions, researchers would pay attentions to the RCS performance. Some works acquire RCS reduction through different ways. The mushroom-like electromagnetic band-gap (EBG) structure is used to reduce the in-band RCS while keep the compact size as the conventional patch antenna [28]. In [29]–[31], the Frequency Selective Surface(FSS) and microstrip resonator are designed in the microstrip antenna to reduce RCS both in and out of the working band. In [32], the superstrate consisting of a polarization rotation reflective surface (PRRS) is designed as a cover of the slot antenna to obtain in-band and out-of-band RCS reduction. Aforementioned PGMs, as well, can be used for significant RCS reduction [1], [3], [4] by guiding, converting or reflecting the incident wave. It could be very attractive to design the PGM antennas with certain properties while the

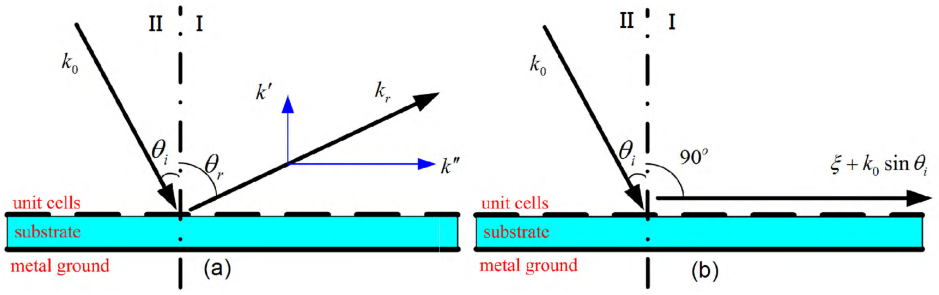

FIGURE 1. (a) anomalous reflection and (b) surface wave coupling of PGMs.

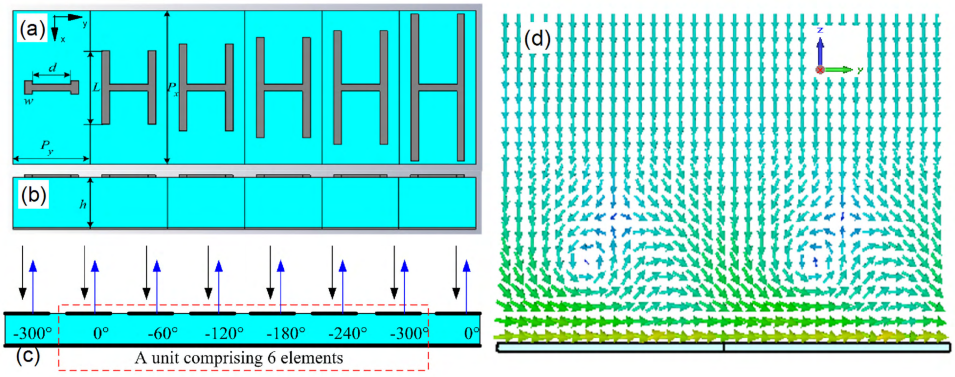

FIGURE 2. (a) top-view and (b) side-view of the unit cell; (c) the reflection phase and (d) the power flow distributions under x-polarized incidence.

RCS reduction be obtained by the antenna itself without any additional structures purposely designed.

In this paper, a low RCS planar antenna utilizing PGM is proposed, which, to the best of our knowledge, has not been studied in depth . A PGM composed of H-shaped sub-elements was designed as an antenna to provide a bridge link between the feeding wave and the radiation wave. A feeding network mediated by a parallel plate waveguide power divider is in the same plane with the PGM. For different frequencies, the wave vectors are different. Thus, the total wave vectors are also different for different frequencies and the beam of the designed metasurface antenna is then controlled by frequency. Because the unit cell of the PGM is non-uniform, it can reflect the cross-polarized incident waves to other directions like diffuse scattering. Thus, the RCS of the metasurface antenna can be significantly reduced.

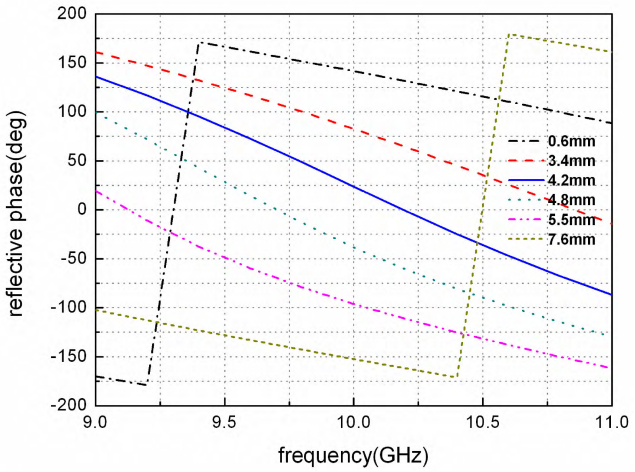

FIGURE 3. Reflection phases of sub-elements with different L.

II. ANTENNA DESIGN

Fig.1 illustrates the schematic diagram for the principle of PGMs. ξ is the phase gradient of the PGM. k_0 and θ_i are the wave number and incident angle of the incident wave. $k_r = k_0$ and θ_r are the wave number and reflection angle of the reflective wave. With a phase gradient ξ along the interface, the reflection will follow the generalized reflection law and $k'' = \xi + k_0 * \sin\theta_i$. Thus, $k'^2 = k_0^2 - k''^2$ and the reflection angle is not equal to the incident angle [22], [23], [27]. When k''^2 is smaller than k_0^2, k' is real and the incident wave will be reflected back to the space with $\tan\theta_r = k''/k'$, as shown in Fig. 1(a). Otherwise, when the phase gradient ξ is big enough to make $k''^2 > k_0^2$, then k' is imaginary and the incident wave will be coupled to a surface wave evanescent in normal direction, as shown in Fig. 1(b).

For a coplanar feeding antenna design, the wave number of the reflective wave should satisfy $k'' = \xi + k_0 \cdot \sin\theta_i > k_0$.

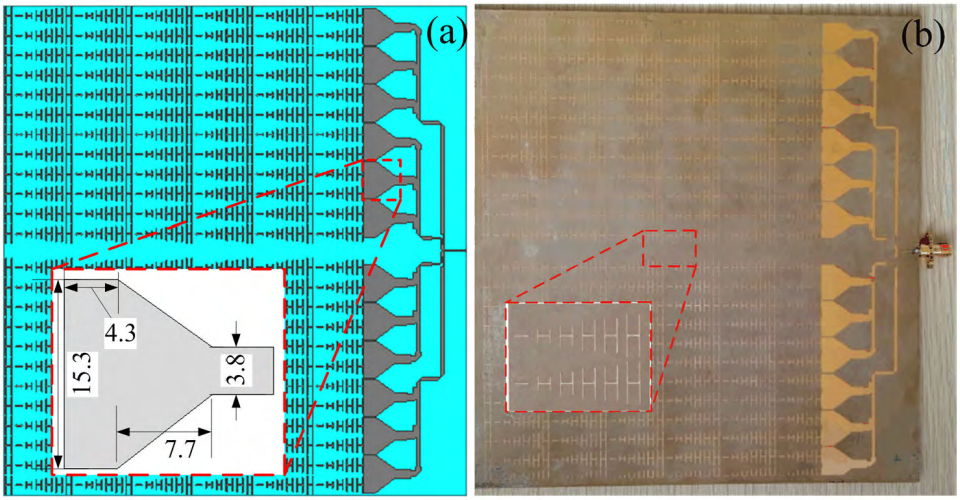

FIGURE 4. (a) The simulation model with geometric parameters by mm and (b) the photograph of the antenna.

Thus, the phase gradient $\xi > k_0 \cdot (1 - \sin\theta_i)$ and the feeding wave from the parallel plate waveguide power divider can be coupled to radiation wave with a direction controlled by ξ.

The overall structure of the PGM unit cell is shown in Fig. 2(a)-(c). Assuming that the electromagnetic wave normally incident to the PGM. The phase gradient ξ is defined as $d\phi/dy$, where $d\phi$ is the phase difference over a distance dy. Here, six H-shaped sub-elements with a metal ground are used to compose a unit cell of the PGM, as shown in Fig. 2(a). The period of each H-shaped sub-element along y direction is P_y. To couple the normal incident wave to surface waves, $\xi = d\phi/dy = \frac{2\pi}{6P_y} > \frac{2\pi}{\lambda_0}$, where λ_0 is the wavelength in the vacuum, should be satisfied. Thus, $P_y < \lambda_0/6$. To realize a linear phase gradient, the phase difference over each sub-element period P_y should be fixed to $\Delta\phi = \pi/3$, as shown in Fig. 2(c).

The permittivity of the substrate is $4.5(1 + 0.025i)$. The central frequency of the proposed antenna is 10 GHz, thus, P_y is selected as 4 mm which is smaller than $\lambda_0/6$. The other geometric parameters are given as $P_x = 8.1$ mm, $w = 0.4$ mm, $d = 1.8$ mm, $h = 2.5$ mm. With different L, the reflection phase of each sub-element can be tuned. To obtain a $\pi/3$ phase difference between each sub-element, L of the six sub-elements are 0.6 mm, 3.4 mm, 4.2 mm, 4.8 mm, 5.5 mm and 7.6 mm respectively. The reflection phases of each sub-element are shown in Fig.3. The phase difference between two adjacent sub-elements is about $\pi/3$ around the central frequency. The unit cell is simulated by a commercial software CST Microwave Studio using unit cell boundary condition and Floquet ports. The simulated power flow distribution is shown in Fig. 2(d), from which one can see that the incident wave is coupled to a surface wave propagating along the phase gradient efficiently. Notably, according to Reciprocity Principle, the PGMs will couple a surface wave propagating opposite to the phase gradient direction to a spatial propagating wave like an antenna radiation.

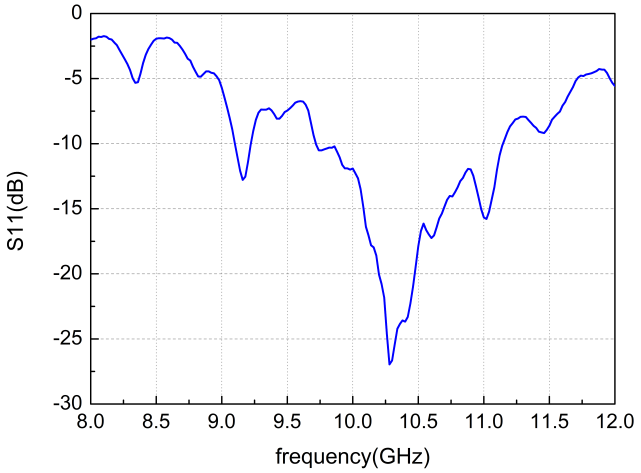

FIGURE 5. The measured S_{11} parameter.

The proposed PGM is realized by the periodical arrangement of 6×24 unit cells. As shown in Fig. 3, from 9.75 GHz to 10.25 GHz, the designed PGM retains a stable phase gradient and can be used as a planar antenna. This PGM antenna was obtained by connecting a typically designed 12 ports parallel plate wave guide power divider to the edge of the PGM, as shown in Fig. 4. Such parallel plate wave guide structure has a good match with surface waves on PGMs and can act as a feeding or receiving structure [10]. The geometric parameters of the parallel plate wave guide power divider is shown in Fig. 4(a). Fig. 4(b) depicts the photograph of the fabricated PGM antenna. The measured S_{11} parameter is shown in Fig. 5.

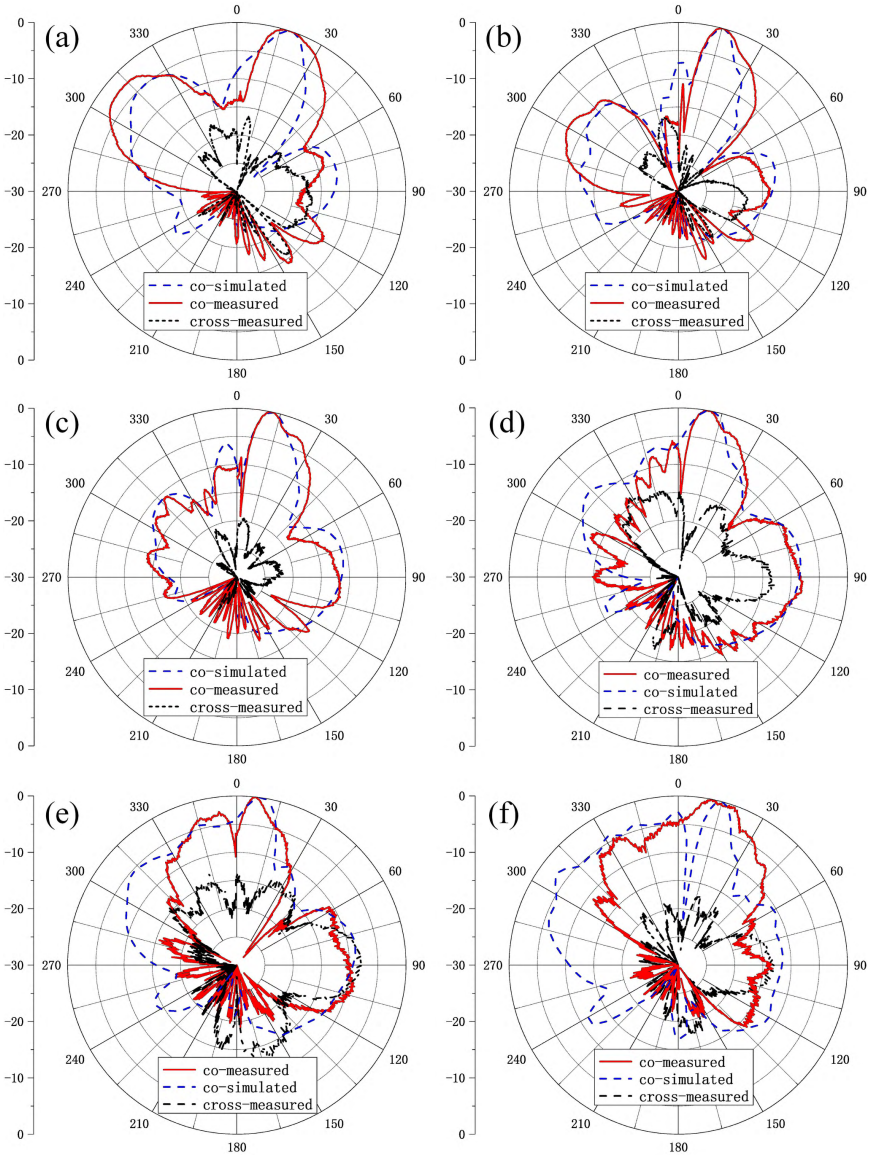

FIGURE 6. Radiation pattern in E-plane at (a) 9.75 GHz, (b) 10 GHz, (c) 10.25 GHz, (d) 10.5 GHz, (e) 10.75 GHz, (f) 11 GHz.

III. RESULTS

A. RADIATION PROPERTY

As shown in Fig.5, the measured results of radiation patterns confirm with the simulated ones. From 9.75 GHz to 10.25 GHz, the return loss is lower than −10 dB. The radiation direction of the antenna is mainly determined by the phase gradient provided by the metasurface.

According to the generalized reflection law, the direction of radiated wave (θ_r) can be governed by [19]

$$\sin\theta_r - \sin\theta_i = \frac{2\pi}{\lambda}\frac{d\phi}{dy} \tag{1}$$

For the proposed antenna, $\theta_i = -90°$ and the radiation direction is thus controlled by the phase gradient ($d\phi/dy$). The phase gradient is designed as $\frac{60°}{4mm} = 1.25k_0$ at 10 GHz. Thus, according to Eq. (1) $\theta_r = 14.5°$. As shown in Fig. 3, the phase gradient is almost invariant from 9.75 GHz to 10.25 GHz. And the calculated and measured radiation directions at different frequencies are listed in table 1. However, θ_r varies with k_0 at different frequencies. The radiation pattern in E-plane and H-plane are shown in Fig. 6 and Fig. 7 respectively. The simulated realized gain of the antenna at 9.75 GHz, 10 GHz, 10.25 GHz, 10.5 GHz, 10.75 GHz and 11 GHz are 15.39 dB, 16.5 dB, 14.01 dB, 11.85 dB, 11.5 dB and 3.93 dB. The borders between each two super cells and edges of the metasurface cause the side lobes. Form 9.75 GHz to 10.25 GHz, the radiation efficiency is about 80% and around 10 GHz the aperture efficiency is about 15% as shown in Fig. 8. Taking the measurement and machining error into account, the measurement results have a good agreement with the theoretical results.

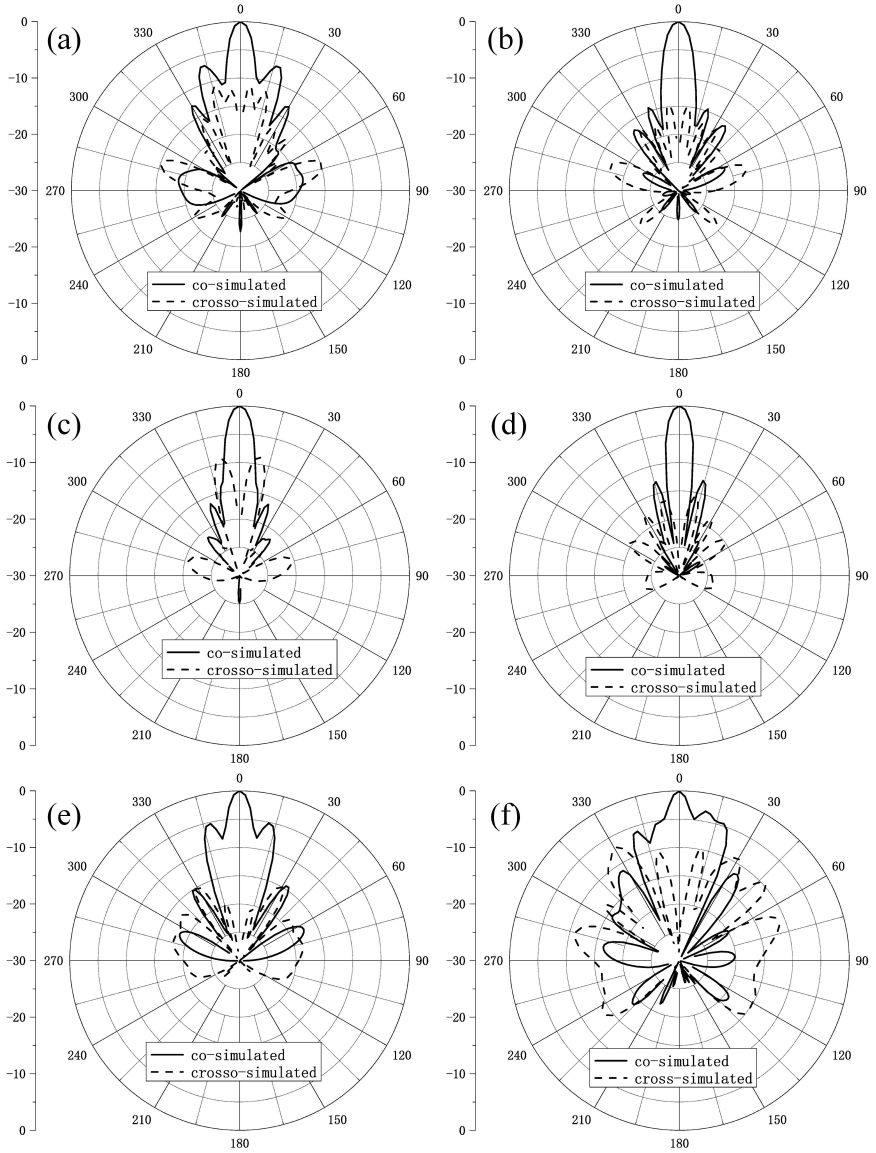

FIGURE 7. Radiation pattern in H-plane at (a) 9.75 GHz, (b) 10 GHz, (c) 10.25 GHz, (d) 10.5 GHz, (e) 10.75 GHz, (f) 11 GHz.

TABLE 1. Radiation directions.

Frequency	9.75 GHz	10 GHz	10.25 GHz
Theory	16.4°	14.5°	12.7°
Measurement	16.6°	15°	13°

B. LOW RCS PROPERTY

As show in Fig. 3, outside the antenna operating band, the sub-elements have an irregular reflective phase difference to each other, which causes diffuse reflections and reduces the monostatic RCS. The reflected phase of each sub-element is listed in the Table. 2. The RCS measurement setup is shown in Fig. 9. Compared to the PEC board in a same size with the proposed PGM, the monostatic RCS is reduced by the PGM under both x-polarized and y-polarized incidences, as shown in Fig. 10. The maximum RCS reduction is more than 22 dB and 30 dB for y-polarized and x-polarized incidences respectively. The phase gradient is along the y-direction under x-polarized incidence. Thus, the proposed antenna has a frequency beam scanning performance along y-direction and the antenna is x-polarized. And the x-polarized incidence in the working frequency band is received by the antenna. For the metasurface alone, under an x-polarized incidence, the scattered wave directs to other angles due to the phase gradient. Notably, the RCS can even be reduced within the antenna operating band with cross-polarization to the antenna polarization. At frequencies ($<$9 GHz and $>$11 GHz), the phase gradient vanished and become random. Thus, the incident wave is diffuse scattered to the space,

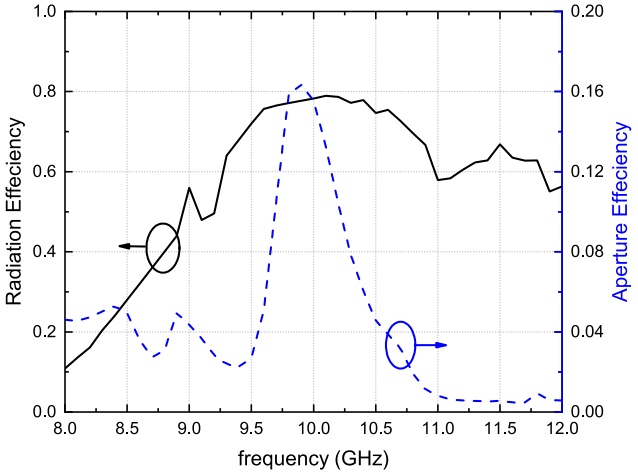

FIGURE 8. The simulated efficiency of the antenna.

TABLE 2. The reflective phase of each element at different frequencies.

L (mm)	0.6	3.4	4.2	4.8	5.5	7.6
9 GHz	170°	161°	136°	99.5°	19.5°	102°
10 GHz	142°	82.7°	23.7°	-38.3°	-96.1°	-152°
11 GHz	88.5°	-14.4°	-86.8°	-130°	-162°	161°

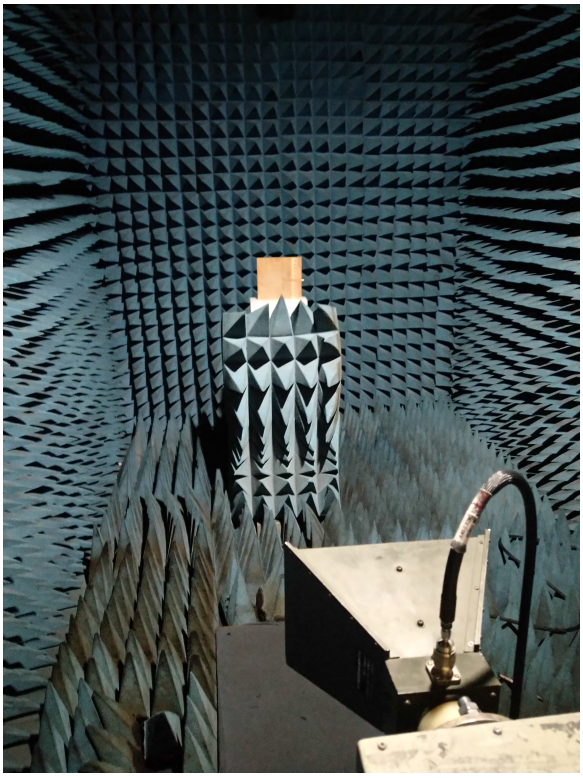

FIGURE 9. The measurement set-up.

which makes it cannot be used as an antenna, but contribute to the RCS reduction. The reference PEC plate is of the same size with the antenna sample.

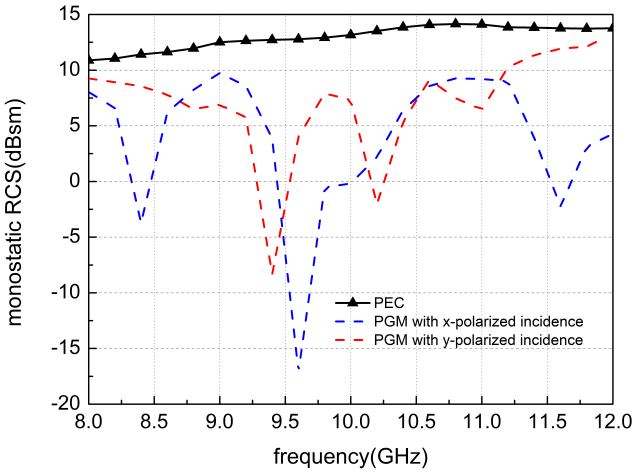

FIGURE 10. Measured monostatic RCS of the PGM and the PEC board.

IV. CONCLUSION

In this paper a frequency scanning PGM antenna was designed with significant RCS reduction. The PGM antenna is excited by a coplanar feeding and thus has a low profile. From 9.75 GHz to 10.25 GHz, the antenna radiation direction scans from 16.4° to 12.7°. The measured results confirm with the simulated results. In addition, the measured maximum RCS reduction is more than 22 dB and 30 dB for *y*-polarized and *x*-polarized incidences respectively.

REFERENCES

[1] J. Chen, J. Zhao, T.-J. Cui, Q. Cheng, and D. S. Dong, "Reduction of radar cross section based on a metasurface," *Prog. Electromagn. Res.*, vol. 146, pp. 71–76, Jan. 2014.
[2] N. M. Estakhri and A. Alù, "Ultra-thin unidirectional carpet cloak and wavefront reconstruction with graded metasurfaces," *IEEE Antennas Wireless Propag. Lett.*, vol. 13, pp. 1775–1778, 2014.
[3] J. Wang *et al.*, "Super-thin cloaks mediated by spoof surface plasmons," *Photonic Nanostruct.*, vol. 10, no. 4, pp. 540–546, Oct. 2012.
[4] Y.-F. Li *et al.*, "Design and experimental verification of a two-dimensional phase gradient metasurface used for radar cross section reduction," *Acta Phys. Sinica*, vol. 63, no. 8, Apr. 2014, Art. no. 084103.
[5] X. Ni, Z. J. Wong, M. Mrejen, Y. Wang, and X. Zhang, "An ultrathin invisibility skin cloak for visible light," *Science*, vol. 349, no. 6254, pp. 1310–1314, Sep. 2015.
[6] A. Forouzmand and A. B. Yakovlev, "Electromagnetic cloaking of a finite conducting wedge with a nanostructured graphene metasurface," *IEEE Trans. Antennas Propag.*, vol. 63, no. 5, pp. 2191–2202, May 2015.
[7] H. M. Bernety A. B. Yakovlev, "Reduction of mutual coupling between neighboring strip dipole antennas using confocal elliptical metasurface cloaks," *IEEE Trans. Antennas Propag.*, vol. 63, no. 4, pp. 1554–1563, Apr. 2015.
[8] J. C. Soric, A. Monti, A. Toscano, F. Bilotti, and A. Alù, "Dual-polarized reduction of dipole antenna blockage using mantle cloaks," *IEEE Trans. Antennas Propag.*, vol. 63, no. 11, pp. 4827–4834, Nov. 2015.
[9] S. Hongyu, Z. Anxue, Z. Shi, L. Jianxing, and J. Yansheng, "Dual-band polarization angle independent 90 degree polarization rotator using twisted electric-field-coupled resonators," *Appl. Phys. Lett.*, vol. 104, no. 3, Jan. 2014, Art. no. 034102.
[10] X. Liu *et al.*, "Frequency-scanning planar antenna based on spoof surface plasmon polariton," *IEEE Antennas Wireless Propag. Lett.*, vol. 16, pp. 165–168, 2016.
[11] K. Zhang, X. Ding, L. Zhang, and Q. Wu, "Anomalous three-dimensional refraction in the microwave region by ultra-thin high efficiency metalens with phase discontinuities in orthogonal directions," *New J. Phys.*, vol. 16, Oct. 2014, Art. no. 103020.

[12] Y. Yuan, X. Ding, K. Zhang, and Q. Wu, "Planar efficient metasurface for vortex beam generating and converging in microwave region," *IEEE Trans. Magn.*, vol. 53, no. 6, Jun. 2017, Art. no. 2500204.
[13] X. Ding, H. Yu, S. Zhang, Y. Wu, K. Zhang, and Q. Wu, "Ultrathin metasurface for controlling electromagnetic wave with broad bandwidth," *IEEE Trans. Magn.*, vol. 51, no. 11, Nov. 2015, Art. no. 2501104.
[14] M. L. N. Chen, L. J. Jiang, and W. E. I. Sha, "Ultrathin complementary metasurface for orbital angular momentum generation at microwave frequencies," *IEEE Trans. Antennas Propag.*, vol. 65, no. 1, pp. 396–400, Jan. 2017.
[15] H. Shi *et al.*, "Gradient metasurface with both polarization-controlled directional surface wave coupling and anomalous reflection," *IEEE Antennas Wireless Propag. Lett.*, vol. 14, pp. 104–107, 2015.
[16] C. Wu, Y. Cheng, W. Wang, B. He, and R. Gong, "Ultra-thin and polarization-independent phase gradient metasurface for high-efficiency spoof surface-plasmon-polariton coupling," *Appl. Phys. Express*, vol. 8, no. 12, Nov. 2015, Art. no. 122001.
[17] J. J. Xu, H. C. Zhang, Q. Zhang, and T. J. Cui, "Efficient conversion of surface-plasmon-like modes to spatial radiated modes," *Appl. Phys. Lett.*, vol. 106, no. 2, Jan. 2015, Art. no. 021102.
[18] J. Wang *et al.*, "High-efficiency spoof plasmon polariton coupler mediated by gradient metasurfaces," *Appl. Phys. Lett.*, vol. 101, no. 20, Nov. 2012, Art. no. 201104.
[19] N. Yu and F. Capasso, "Flat optics with designer metasurfaces," *Nature Mater.*, vol. 13, no. 2, pp. 139–150, Jan. 2014.
[20] S. Sun *et al.*, "High-efficiency broadband anomalous reflection by gradient meta-surfaces," *Nano Lett.*, vol. 12, no. 12, pp. 6223–6229, Dec. 2012.
[21] L. Huang *et al.*, "Dispersionless phase discontinuities for controlling light propagation," *Nano Lett.*, vol. 12, no. 11, pp. 5750–5755, Nov. 2012.
[22] N. Yu *et al.*, "Light propagation with phase discontinuities: Generalized laws of reflection and refraction," *Science*, vol. 334, no. 6054, pp. 333–337, Oct. 2011.
[23] H. Shi, J. Z. Chen, S. Xia, A. Zhang, J. Wang, and Z, Xu, "Polarization-insensitive unidirectional spoof surface plasmon polaritons coupling by gradient metasurface," *Chin. Phys. B*, vol. 25, no. 7, Jul. 2016, Art. no. 078105.
[24] H. Li, G. Wang, H.-X. Xu, T. Cai, and J. Liang, "X-band phase-gradient metasurface for high-gain lens antenna application," *IEEE Trans. Antennas Propag.*, vol. 63, no. 11, pp. 5144–5149, Nov. 2015.
[25] Y. Fan *et al.*, "Frequency scanning radiation by decoupling spoof surface plasmon polaritons via phase gradient metasurface," *IEEE Trans. Antennas Propag.*, vol. 66, no. 1, pp. 203–208, Jan. 2018.
[26] T. Cai *et al.*, "Ultra-thin polarization beam splitter using 2-D transmissive phase gradient metasurface," *IEEE Trans. Antennas Propag.*, vol. 63, no. 12, pp. 5629–5636, Dec. 2015.
[27] S. Sun, Q. He, S. Xiao, Q. Xu, X. Li, and L. Zhou, "Gradient-index meta-surfaces as a bridge linking propagating waves and surface waves," *Nature Mater.*, vol. 11, no. 5, pp. 426–431, May 2012.
[28] W. Xu, J. Wang, M. Chen, Z. Zhang, and Z. Li, "A novel microstrip antenna with composite patch structure for reduction of in-band RCS," *IEEE Antennas Wireless Propag. Lett.*, vol. 14, pp. 139–142, Sep. 2014.
[29] Y. Liu, Y. Hao, H. Wang, K. Li, and S. Gong, "Low RCS microstrip patch antenna using frequency-selective surface and microstrip resonator," *IEEE Antennas Wireless Propag. Lett.*, vol. 14, pp. 1290–1293, Feb. 2015.
[30] J. Xue, W. Jiang, and S. Gong, "Wideband RCS reduction of microstrip antenna based on 2.5-dimension miniaturized frequency selective surface," in *Proc. IEEE 5th Asia–Pacific Conf. Antennas Propag. (APCAP)*, Jul. 2016, pp. 209–210.
[31] Y. Jia, Y. Liu, H. Wang, and S. Gong, "Low RCS microstrip antenna using polarisation-dependent frequency selective surface," *Electron. Lett.*, vol. 50, no. 14, pp. 978–979, Jul. 2014.
[32] Y. Jia, Y. Liu, W. Zhang, J. Wang, and G. Liao, "In-band radar cross section reduction of slot array antenna," *IEEE Access*, vol. 6, pp. 23561–23567, Jan. 2018.

BO LI received the B.S. degree in electronic and information engineering and the M.S. degree in electromagnetic field and microwave technology from Xi'an Jiaotong University, in 2010 and 2012, respectively. He is currently pursuing the Ph.D. degree in radio physics with the China Academy of Engineering Physics, Mianyang, China.

His research interests include metamaterials, antennas on platform, ultra-wideband antenna, and arrays.

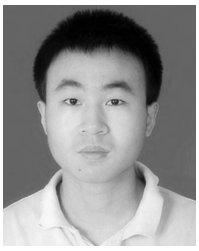

XIAOBO LIU received the B.S. degree in information engineering and the Ph.D. degree in electronics science and technology from Xi'an Jiaotong University, Xi'an, China, in 2014 and 2018, respectively.

His current research interests include metasurface, the design of antenna, microwave circuit, and electromagnetic theory.

HONGYU SHI was born in 1987. He received the M.S. degree in information engineering from Dalian Maritime University, Dalian, China, in 2010, and the Ph.D. degree in electronic science and technology from Xi'an Jiaotong University, Xi'an, China, in 2015.

He is currently a Lecturer with Xi'an Jiaotong University. His current research interests include metamaterials and antennas.

CHUN YANG received the B.S. and M.S. degrees in radio engineering from Sichuan University, in 1995 and 1998, respectively, and the Ph.D. degree in radio physics from Lomonosov Moscow State University, in 2007. He is currently a Research Fellow with the China Academy of Engineering Physics, Mianyang, China. He has published more than 20 academic papers.

QI CHEN was born in Chongqing, China, in 1981. He received the B.S. degree in remote sensing techniques and instrument and the M.S. degree in electromagnetic and microwave techniques from Xidian University, Xi'an, China, in 2003 and 2007, respectively, and the Ph.D. degree in radio physics from the China Academy of Engineering Physics (CAEP), Mianyang, China, in 2017.

He joined the Institute of Electronic Engineering, CAEP, in 2007. His research interests include mmW/terahertz antennas, photocrystal, and metamaterials.

ANXUE ZHANG received the B.S. degree in electrical and electronics engineering from Henan Normal University, Xinxiang, China, in 1996, and the M.S. and Ph.D. degrees in electromagnetic and microwave engineering from Xi'an Jiaotong University, Xi'an, China, in 1999 and 2003, respectively. He is currently a Professor with Xi'an Jiaotong University.

His current research interests include antenna and electromagnetic wave propagation, RF and microwave circuit design, array signal processing, and metamaterials.